

Online Decorrelation of Humidity and Temperature in Chemical Sensors for Continuous Monitoring

Ramon Huerta^a, Thiago Mosqueiro^a, Jordi Fonollosa^{b,c}, Nikolai F Rulkov^a, Irene Rodriguez-Lujan^d

^a*BioCircuits Institute
University of California, San Diego
La Jolla, CA 92093, USA*

^b*Institute for Bioengineering of Catalunya,
Baldiri Reixac, 4-8,
08028 Barcelona, Spain*

^c*Department of Engineering: Electronics,
Universitat de Barcelona,
Martí i Franquès, 1,
08028 Barcelona, Spain*

^d*Dpto. de Ingeniería Informática, Escuela Politécnica Superior,
Universidad Autónoma de Madrid,
Calle Francisco Tomás y Valiente, 11,
28049 Madrid, Spain*

Abstract

A method for online decorrelation of chemical sensor signals from the effects of environmental humidity and temperature variations is proposed. The goal is to improve the accuracy of electronic nose measurements for continuous monitoring by processing data from simultaneous readings of environmental humidity and temperature. The electronic nose setup built for this study included eight metal-oxide sensors, temperature and humidity sensors with a wireless communication link to external computer. This wireless electronic nose was used to monitor air for two years in the residence of one of the authors and it collected data continuously during 537 days with a sampling rate of 1 samples per second. To estimate

Email addresses: rhuerta@ucsd.edu (Ramon Huerta), tmosqueiro@ucsd.edu (Thiago Mosqueiro), jfonollosa@ibecbarcelona.eu (Jordi Fonollosa), nrulkov@ucsd.edu (Nikolai F Rulkov), irene.rodriquez@uam.es (Irene Rodriguez-Lujan)

the effects of variations in air humidity and temperature on the chemical sensors signals, we used a standard energy band model for an n-type metal-oxide (MOX) gas sensor. The main assumption of the model is that variations in sensor conductivity can be expressed as a nonlinear function of changes in the semiconductor energy bands in the presence of external humidity and temperature variations. Fitting this model to the collected data, we confirmed that the most statistically significant factors are humidity changes and correlated changes of temperature and humidity. This simple model achieves excellent accuracy with a coefficient of determination R^2 close to 1. To show how the humidity-temperature correction model works for gas discrimination, we constructed a model for online discrimination among banana, wine and baseline response. This shows that pattern recognition algorithms improve performance and reliability by including the filtered signal of the chemical sensors.

Keywords: electronic nose, chemical sensors, humidity, temperature, decorrelation, wireless e-nose, MOX sensors, energy band model, home monitoring

1. Introduction

Conductometric chemical sensors are known to be very sensitive to humidity levels in the environment [1–11]. This cross-sensitivity challenges the tasks of identification and quantification of volatiles in uncontrolled scenarios. For example, electronic noses can be used for human monitoring purposes [12–17]. In fact, they have been successfully used to quantify the number of people working in a space-craft simulator [18]. In this case, it is likely that the primary signal used by the algorithm to estimate the number of people present at some given time is the humidity level in the chamber. If we filter the sensor responses by the humidity and temperature changes, a clearer chemical signature of the chamber can be obtained, and this can facilitate more complex monitoring tasks like identifying individuals [19]. A possible solution to this sensitivity problem is the design of a special sensing chamber that controls humidity and delivers the gas to the sensors under predefined conditions [20–22, 18, 8]. Such preconditioning chambers are effective for signal improvement, but their use increases the costs of electronic nose design for applications in continuous monitoring of the environment [14]. A different approach is to build a model that predicts the changes in the sensor conductance as a function of humidity and temperature variations [5, 8, 23, 24].

The prevailing phenomenological model of sensor sensitivity is that the ratio of the sensor resistance depends on a power law of the gas concentration [25]. The model provides accurate predictions when the gas is known and under controlled conditions. However, it is rendered inaccurate with changes in the environment. Correction methods based on artificial neural networks [8] using present and past values of the input features are proven to be successful despite lacking an explanation of the underlying processes. Fundamental models, on the other hand, can capture the dynamical changes of resistance under humidity variations accurately [23]. In these models, the number of parameters is not large, but the model parameters depend on the presented gas to the sensors. Therefore, in continuous monitoring systems, where there can be a complex mixture of gases present in the air, it is indeed challenging to make proper corrections on the sensor readings based on humidity and temperature variations.

29 In this work, we propose an online methodology to subtract the changes driven by humid-
30 ity and temperature from the MOX sensor responses, and demonstrate that this procedure
31 enhances the performance of pattern recognition algorithms in discriminating different chem-
32 ical signatures. We first develop a model based on the energy bands of n-type semiconductors
33 that is suitable for low-power micro-controllers (Texas Instruments MSP430F247). We then
34 make use of the predictions of this model to subtract changes expected to be due to humidity
35 and temperature variation. Using a wireless electronic nose composed of 8 MOX sensors,
36 we collected 537 days of data in the residence of one of the authors and showed that our
37 model is capable of predicting all MOX sensors with a coefficient of determination R^2 larger
38 than 0.9. Because the electronic nose was subject to several unpredictable conditions (house
39 cleaning, wireless connectivity issues, etc), this data set represents a wide variety of events
40 present in home monitoring scenarios. To evaluate the impact to online discrimination of
41 volatiles identities, we created a small data set consisting of exposing the electronic nose
42 to two distinct stimuli: wine and banana. We show that the discrimination performance is
43 significantly enhanced using the decorrelated data combined with the raw time series. This
44 is a crucial task for any electronic nose system if one wants to characterize or detect events
45 based on their chemical signatures in the presence of varying environmental conditions.

46 **2. Example of sensors correlation with humidity and temperature**

47 In Fig. 1, we show a representative example of the humidity problem using chemical
48 sensors for continuous monitoring purposes. The electronic nose in our setup is composed of
49 8 metal oxide (MOX) sensors, along with temperature and humidity sensors. Such platform
50 was previously used in our wind tunnel studies to identify 10 gases at different locations [26].
51 As a result of this previous investigation, we know that we can discriminate between gases
52 accurately, and estimate gas concentrations in the ppm range [27]. The time series shown
53 in Fig. 1 were obtained in October 2014 in a regular working day, in the residence of one of
54 the authors.

55 The top panel shows the humidity levels throughout a complete day, where the x -axis
56 indicates the hour of the day. For example, the first rise in humidity at about 5:30 AM

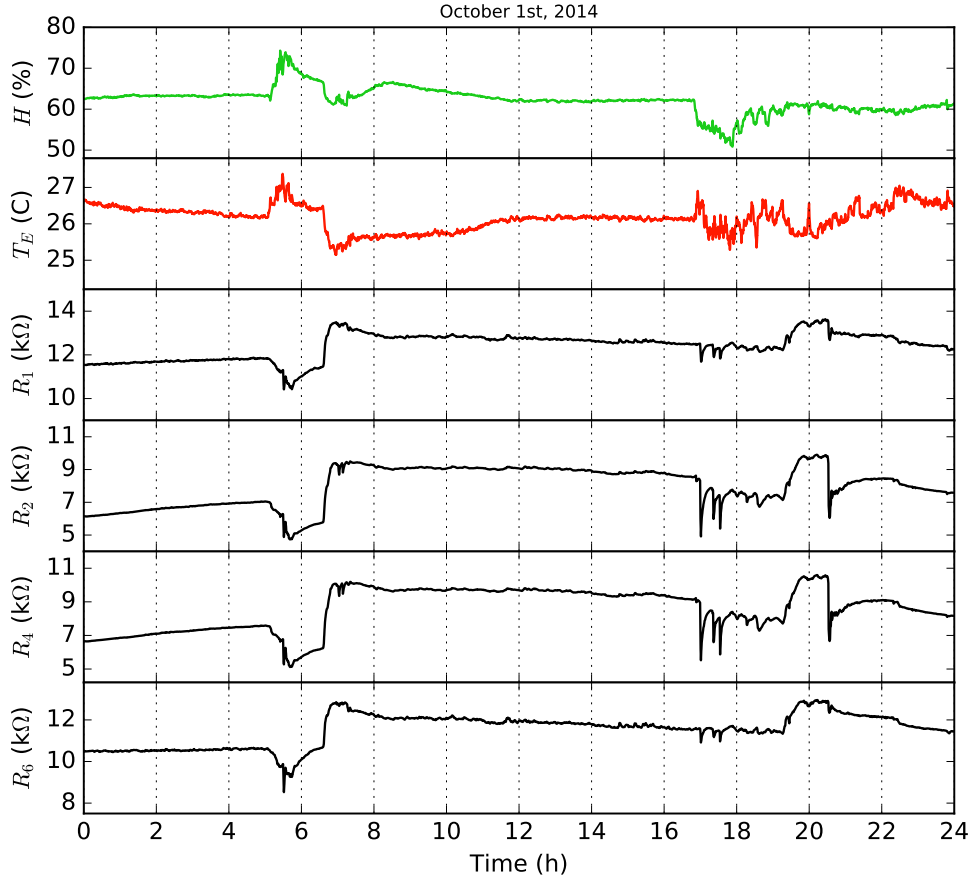


Figure 1: Illustrative example of recording during one day using the wireless electronic nose composed of 8 MOX sensors, including a humidity and temperature sensor. The first panel presents the humidity values, the second panel is the external temperature, and then resistance values for 4 different MOX sensors in the board.

57 corresponds to the morning shower. The sudden drop in humidity at about 6:30 AM indicates
 58 opening the bathroom window, and the changes observed at 5 PM are associated with the
 59 moment at which the family was returning home and the door to the backyard was being
 60 opened. The second panel presents the temperature of the electronic nose location that we
 61 denote by T_E to differentiate it from the temperature of the sensor heater, T . This residence
 62 did not have any air conditioning system or heater operating during this period.

63 It is clear from this graph that the environmental changes in humidity and temperature
 64 are often correlated. The measured resistance values of the MOX sensors are presented in the

Sensor type	Number of units	Target gases
TGS2611	1	Methane
TGS2612	1	Methane, Propane, Butane
TGS2610	1	Propane
TGS2600	1	Hydrogen, Carbon Monoxide
TGS2602	2	Ammonia, H ₂ S, Volatile Organic Compounds (VOC)
TGS2620	2	Carbon Monoxide, combustible gases, VOC

Table 1: Sensor devices selected for the wireless electronic nose (provided by Figaro Inc.)

65 four bottom panels. Although the sensor board is made of 8 MOX sensors, here we present
66 recordings of only 4 of them because the remaining sensors are highly correlated with those
67 shown. Changes in the sensors resistance are strongly affected by changes in humidity and
68 temperature, as expected from the extensive literature on the topic [1–11]. Nevertheless, the
69 whole data set also includes examples where MOX sensor changes cannot be explained only
70 in terms of variations in humidity and temperature as there also exist chemical variations in
71 the environment that have effects on sensors’ responses. As exposed before, our goal is to
72 find a way to decorrelate the MOX sensors from humidity and temperature, and show that
73 this improves pattern recognition tasks such as discrimination of gas identity.

74 3. Design of the wireless electronic nose

75 In this section, we describe the electronic nose designed for home monitoring purposes.
76 The sensor array is based on eight metal oxide gas sensors provided by Figaro Inc. The
77 sensors are based on six different sensitive surfaces, which are selected to enhance the sys-
78 tem selectivity and sensitivity. Table 1 shows the selected sensing elements along with the
79 corresponding target compounds. In order to control the variability between the sensing
80 elements and increase the flexibility of the sensing platform, the operating temperature of
81 the sensors can be adjusted by applying a voltage to the built-in, independently reachable
82 heating element available in each sensor. The humidity and temperature sensors are inte-
83 grated in the board using the Sensirion SHT75. The device is very similar to the M-Pod [24],
84 except that ours is directly powered by any electrical outlet to record continuously over long
85 periods of time.

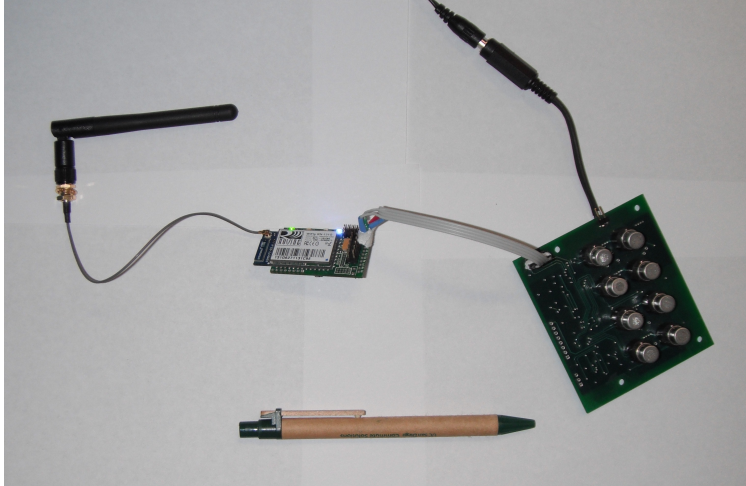


Figure 2: The electronic nose made of the sensor board (right) and a wireless communication board.

86 The sensor array is integrated with a customized board that includes a microprocessor
87 MSP430F247 (Texas Instruments Inc.). In Fig. 2 we show the operating electronic nose. The
88 microcontroller was programmed to perform the following actions: i) Continuous data collec-
89 tion from the eight chemical sensors through a 12-bit resolution analog-to-digital converter
90 (ADC) device at a sampling rate of 100 Hz; ii) Control of the sensor heater temperature by
91 means of 10 ms period and 6 V amplitude Pulse-Width-Modulated (PWM) driving signals;
92 iii) A two-way communication with another device to transmit the acquired data from the
93 sensors and control the voltage in the sensors' heaters. The sensor board provides serial data
94 communication to another device via either a USB and/or a 4-pin connector (Tx, Rx, Gnd,
95 Vcc).

96 A wireless communication module acts as a bridge between the MSP430F247 microcon-
97 troller and the network. The communication with the MSP430F247 microcontroller is done
98 via the UART port, whereas the communication with the network is performed wirelessly.
99 The board is based on a WiFly RN-131G radio module included in a RN-134 SuRF board
100 (Roving Networks Inc). The WiFly module incorporates a 2.4GHz radio, processor, full
101 TCP/IP stack, real-time clock, FTP, DHCP, DNS, and web server.

102 The module can be accessed via a RS-232 serial port (9600 default baud rate) or a 802.11
103 wireless network so that its configuration can be modified. The wireless communication

104 module is configured such that it accepts UDP and TCP connections, the baud rate of
 105 the microprocessor is set to 115200 so that it can exchange data with the MSP430F247
 106 microcontroller, and working with an external 4" reverse polarity antenna to increase the
 107 power of the transmission.

108 4. Online model for sensors response

109 An energy band model for n-type semiconductors describes the changes in the resistance
 110 of the sensor before exposure, R_I , and after exposure, R_F , as a nonlinear expression of the
 111 changes in the semiconductor's energy bands [1, 2]. Energy bands changes depend on varia-
 112 tions in humidity and gas external temperature, which modulates the overall transduction.
 113 If we denote by $\Delta\Phi = \Phi_F - \Phi_I$ the work function change computed as the difference between
 114 the work function after and before exposure, and we express the electron affinity change as
 115 $\Delta\chi = \chi_F - \chi_I$, the overall transduction can be expressed (following [2]) as:

$$\ln\left(\frac{R_F}{R_I}\right) = \frac{1}{k_B T} (\Delta\Phi - \Delta\chi), \quad (1)$$

116 where k_B is the Boltzmann constant, and T is the sensor operating temperature controlled by
 117 the built-in sensor heater. The sensor temperature is not constant because it is modulated
 118 by the external temperature, T_E . To be able to build a basic model to be fitted to the
 119 data, we make the following assumptions. We assume that relative changes in the external
 120 humidity, $\Delta H = h$, and changes in external temperature, $\Delta T_E = t$, are small enough. We
 121 also assume that the chemical content remains unchanged during the environmental changes.
 122 This assumption is important because it is known that humidity changes induce nonlinear
 123 changes in the energy depending on the chemical agent (see [4]). Under these assumptions,
 124 we can rewrite the transduction in equation 1 as

$$\ln\left(\frac{R_F}{R_I}\right) = \frac{1}{k_B(T + \mu t)} (\Delta\Phi(h) - \Delta\chi(h)), \quad (2)$$

125 where $\mu > 0$ is a dimensionless factor that reflects the impact of the external temperature
 126 into the sensor.

127 Because the sensor board is based on a Texas Instruments MSP430F247 micro-controller,
 128 which can only perform simple mathematical operations, we now consider in equation 2 terms
 129 up to second order in ΔH and ΔT . This removes most of the non-linearities from equation
 130 2, but without oversimplifying the model. We investigate the validity of this approximation
 131 in section 5 in each of the sensors separately. Thus,

$$\ln\left(\frac{R_F}{R_I}\right) = \left(\frac{1}{k_B T} - \frac{\mu}{k_B T^2}t + \frac{\mu^2}{k_B T^3}t^2 + O(t^3)\right) \times$$

$$\left(\Delta\Phi(0) - \Delta\chi(0) + \left[\frac{\partial\Delta\Phi}{\partial h}\Big|_{h=0} - \frac{\partial\Delta\chi}{\partial h}\Big|_{h=0}\right]h + \frac{1}{2}\left[\frac{\partial^2\Delta\Phi}{\partial h^2}\Big|_{h=0} - \frac{\partial^2\Delta\chi}{\partial h^2}\Big|_{h=0}\right]h^2 + O(h^3)\right). \quad (3)$$

132 Note that $\Delta\Phi(0) - \Delta\chi(0) = 0$ because there are not changes in humidity and temperature
 133 on our sampling time scale. The simplified model is

$$\ln\left(\frac{R_F}{R_I}\right) = \frac{1}{k_B T} \left[\frac{\partial\Delta\Phi}{\partial h}\Big|_{h=0} - \frac{\partial\Delta\chi}{\partial h}\Big|_{h=0}\right]h + \frac{1}{2k_B T} \left[\frac{\partial^2\Delta\Phi}{\partial h^2}\Big|_{h=0} - \frac{\partial^2\Delta\chi}{\partial h^2}\Big|_{h=0}\right]h^2$$

$$- \frac{\mu}{k_B T^2} \left[\frac{\partial\Delta\Phi}{\partial h}\Big|_{h=0} - \frac{\partial\Delta\chi}{\partial h}\Big|_{h=0}\right]ht. \quad (4)$$

134 Therefore, we fit the following model to the data

$$\ln\left(\frac{R_F}{R_I}\right) = \beta_1\Delta H + \beta_2(\Delta H)^2 + \beta_3\Delta H\Delta T_E, \quad (5)$$

135 where

$$\beta_1 = \frac{1}{k_B T} \left[\frac{\partial\Delta\Phi}{\partial h}\Big|_{h=0} - \frac{\partial\Delta\chi}{\partial h}\Big|_{h=0}\right]$$

$$\beta_2 = \frac{1}{2k_B T} \left[\frac{\partial^2\Delta\Phi}{\partial h^2}\Big|_{h=0} - \frac{\partial^2\Delta\chi}{\partial h^2}\Big|_{h=0}\right]$$

$$\beta_3 = -\frac{\mu}{k_B T^2} \left[\frac{\partial\Delta\Phi}{\partial h}\Big|_{h=0} - \frac{\partial\Delta\chi}{\partial h}\Big|_{h=0}\right].$$

Sensor	RMS	R^2	$\beta_1 (\beta_1/se(\beta_1))$	$\beta_2 (\beta_2/se(\beta_2))$	$\beta_3 (\beta_3/se(\beta_3))$	β_3/β_1
1	0.06	1.00	-0.0044 (-128.14)*	0.00014 (38.40)*	0.0110 (58.41)*	-2.61
2	0.12	1.00	-0.0110 (-186.04)*	0.00034 (54.11)*	0.0240 (71.75)*	-2.21
3	0.12	1.00	-0.0110 (-187.12)*	0.00034 (53.57)*	0.0230 (69.60)*	-2.18
4	0.14	1.00	-0.0110 (-190.95)*	0.00033 (55.31)*	0.0230 (73.06)*	-2.19
5	1.24	0.98	-0.0056 (-41.48)*	0.00018 (12.23)*	0.0086 (11.15)*	-1.54
6	0.48	0.99	-0.0039 (-104.94)*	0.00012 (30.29)*	0.0071 (33.71)*	-1.84
7	2.06	0.90	-0.0070 (-99.24)*	0.00022 (28.94)*	0.0095 (23.57)*	-1.36
8	2.09	0.91	-0.0057 (-70.75)*	0.00020 (22.94)*	0.0029 (6.43)*	-0.52

Table 2: Results of fitting the model defined in equation (5). The Root Mean Square (RMS) of the error in the predictions always remained below 3.0, and the coefficient of determination R^2 was always above 0.9. We also show the coefficients β_1 , β_2 , and β_3 fitted for each sensor, along with their signal-to-noise ratio ($se(X)$ stands for standard error of X). All β parameters are statistically significant (indicated with a *), with a p -value below 10^{-10} .

Thus, our model has only three parameters to be fitted: β_1 , β_2 and β_3 . In particular, β_1 and β_3 have opposite sign and they are related by $\beta_3/\beta_1 = -\mu/T$. This means that the ratio $|\beta_3/\beta_1|$ becomes smaller with increasing sensor temperature.

5. Results

We fit the model defined in equation (5) to data of 537 days (from Feb 17, 2013 until June 5 2015) by down-sampling the time series to one data point per minute and per sensor. Heaters for sensors 1-4 are always kept at the same operating voltage, while sensors 5 to 8 are controlled under a protocol that guarantees that the sensor responses always remain within a the same range of values. Results summarized in Table 2 prove the effectiveness and statistical significance of the energy band model: the accuracy rates achieved by the model, measured by the coefficient of determination R^2 , are above 90% for all sensors, and all the model coefficients are statistically significant. Sensors with a fixed heater temperature (i.e., sensors 1-4) outperformed sensors that operate with their heater temperature actively changed (i.e., sensors 5-8). In the worst case (sensor 8), the difference in R^2 is close to 10%. This probably suggests that higher order terms become important in the approximation of equation (3) when the heater temperature is actively changed. Moreover, as predicted by equation (4), the parameters β_1 and β_3 have opposite signs for all the sensors in the electronic

153 nose. The ratios β_3/β_1 estimated for the eight MOX sensors by our fitting (see Table 2) are
 154 consistent with the voltage applied on the sensors’ heaters: obtained ratios for sensors 1-4 are
 155 similar as the sensors are kept under the same heating conditions, and ratios for sensors 5-8
 156 are lower as, due to the active temperature control, they tend to be at higher temperature.

157 To filter the signal components due to changes in humidity and temperature, we subtract
 158 the model prediction in equation (5) from the raw sensor output. This operation is recognized
 159 as a method that searches signals independent of environmental conditions [28]. This is
 160 typically the case for continuous monitoring devices that are not intended to measure the
 161 concentration of a particular gas. The resulting signal is

$$R_i^*(t) = R_i(t) - \bar{R}_i(t) = R_i(t) - R_i(t-1)e^{(\beta_{1i}\Delta H + \beta_{2i}(\Delta H)^2 + \beta_{3i}\Delta H\Delta T_E)}, \quad (6)$$

162 where R_i denotes the resistance values of the sensor i , and β_{1i} , β_{2i} , and β_{3i} are the adjusted
 163 values for β_1 , β_2 , and β_3 for the i -th sensor. In Fig. 3, we show the result of applying this
 164 transformation on sensor 1. On the left panel, we present the humidity, temperature, and
 165 sensor output. After applying the transformation, the decorrelated output of the sensor is
 166 shown on the right panel. The sensor drift due to the temperature and humidity changes
 167 is filtered out. However, because we are subtracting from the sensors signal $R_i(t)$ their
 168 predicted value $\bar{R}_i(t)$ according to our model, the resulting filtered signal $R_i^*(t)$ often has
 169 zero mean and the relationship among the sensors is partially lost. This is important for gas
 170 discrimination [26], and we deal with this issue in section 6.

171 5.1. Parameter Stability

172 To test the stability of the parameters over time, we trained the model over a short period
 173 of time of 3 months of data and tested its performance in the following month (i.e., forward
 174 testing methodology). In Fig. 4, we show the time evolution of the model performance
 175 and parameters β of sensor 1 based on humidity and temperature changes. The window
 176 of 3 months was chosen in order to guarantee $R^2 > 0.9$ for all sensors throughout the year
 177 (Fig. 5a) and to avoid longer time scales, where sensor drifting and seasonal changes in

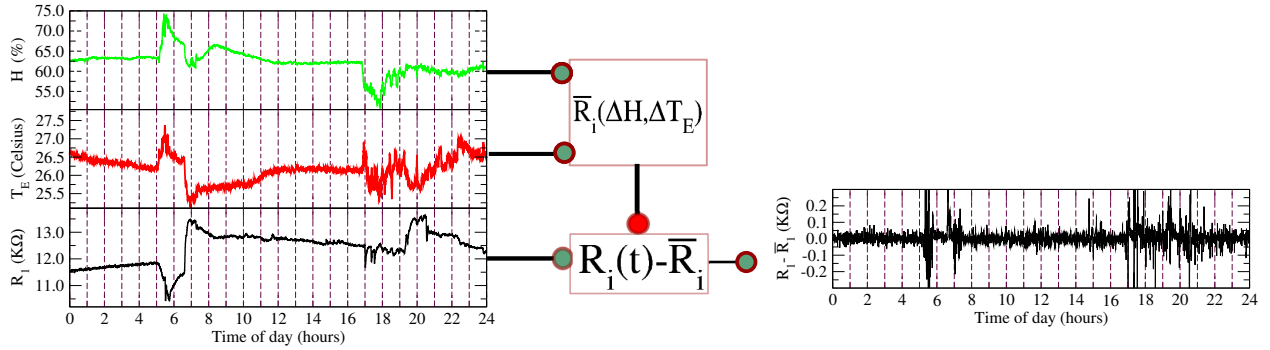


Figure 3: Result of applying the humidity and temperature filter provided by equation (5) on sensor 1. First, the resistance is predicted using the variation in humidity, and then this predicted resistance is subtracted from the original signal

178 the environment may influence sensors response. We also show the histogram of all values
 179 assumed by β parameters throughout this period (Fig. 5b–d).

180 Finally, the model is robust to failures in the sensors due to number of reasons. For
 181 instance, in some instances the electronic nose stopped transmitting due issues in the wire-
 182 less connectivity; in other events, sensors were displaced from their location during house
 183 cleaning, and stopped working. Because algorithms need to be as robust as possible given
 184 the uncontrolled conditions under which they operate, our R^2 already takes it into account.
 185 In summary, there are many possible reasons in daily operations that hinder the operation
 186 of the electronic nose, and they reproduce uncontrolled conditions that such sensors face.

187 5.2. Sampling rate

188 Another important question is determining an acceptable sampling rate on the electronic
 189 nose to be able to filter the humidity and the temperature. We estimate the effect in terms
 190 of regression accuracy of different sampling rates by computing the average R^2 values for all
 191 the sensors modifying the sampling period from 5 to 500 seconds. In Fig. 6, we can see that
 192 beyond the 2 minute sampling period, the filter performance drops below 0.9. Beyond this
 193 point, the approximations made in the band-based model in equations (3-4) fail.

194 Faster sampling rates may still be required to implement for some strategies that use
 195 sensor heater control in an active manner [29] or in fast changing environments. However,
 196 further work is still needed to consider highly ventilated scenarios in which temperature

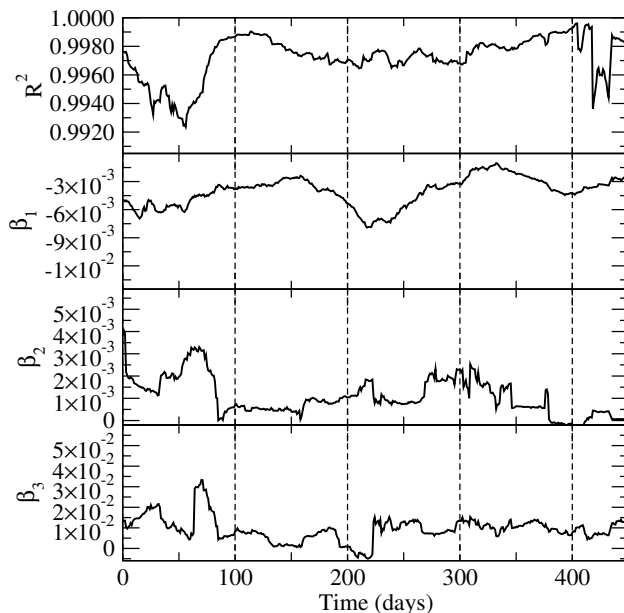


Figure 4: Time evolution of the out-of-sample performance measured by evaluating R^2 on the first sensor of the electronic nose. The three bottom panels represent the evolution of the parameters, β_1 , β_2 and β_3 of the model over time.

197 and humidity change in time at the same rate as the atmosphere chemical composition..
 198 Comparatively, an empirical approach can be found in [24], where a similar model is fitted to
 199 a linear dependence on temperature and humidity, but not on the changes of the temperature
 200 and humidity.

201 6. Impact on online discrimination of gas identity

202 To investigate whether a predictive model can potentially benefit from filtering tempera-
 203 ture and humidity sensors, we constructed a data set from recordings of two distinct stimuli:
 204 wine and banana (Fig. 7). We compared the impact of using the raw data and the filtered
 205 data in terms of classification performance when discriminating among presence of banana,
 206 wine and lack of stimulus (i.e., background activity). Signals recorded with banana or wine
 207 evoked different responses in the sensors. In particular, responses to banana were often
 208 weaker and returned to the baseline activity much faster than those of wine (compare for
 209 instance R_4 in Fig. 7). Rather than using the particular chemical signatures of compounds
 210 from bananas and wines, our goal is to construct a model that learns to predict presence of

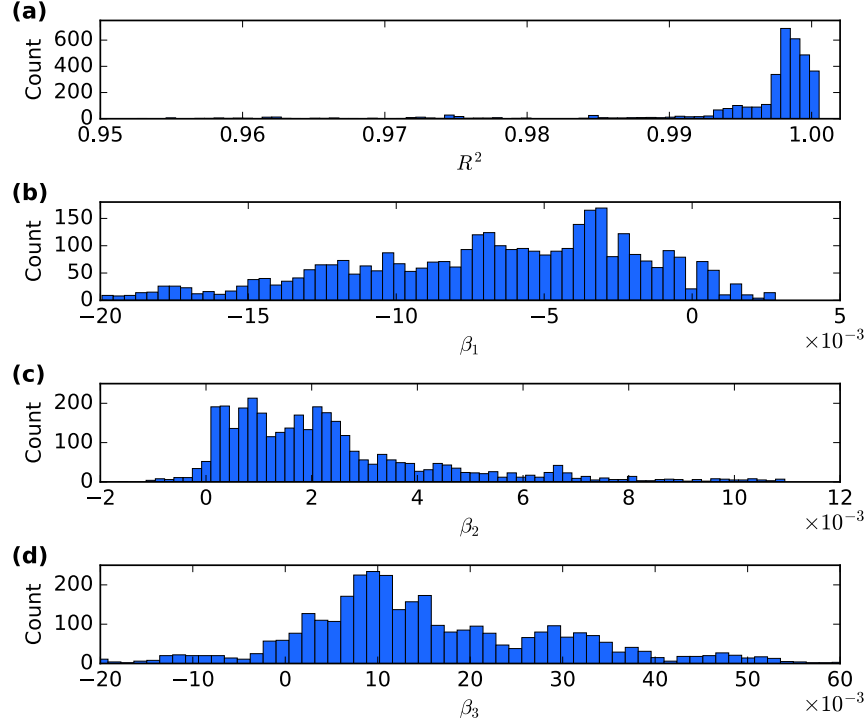


Figure 5: Histograms of performance R^2 (a) and values of β parameters (b-d) for all the sensors using 3 months of training and testing in the following month.

211 banana/wine based on the multivariate response of the sensors. The chemical signature of
 212 bananas changes, for instance, as they ripen [30], and wine’s signature depends on alcohol
 213 content (ethanol), origin of the grape, among other factors [31, 32]. Thus, our approach
 214 attempts at building a model that does not rely on wine type and banana ripeness.

215 These data were collected over the course of 2 months by placing a sample of either a
 216 banana or wine next to the electronic nose for a period of time ranging from 10 minutes to 1
 217 hour. Baseline signals were taken from 2PM to 3PM to avoid additional noise due to home
 218 activity. The time of the day when the stimulus was presented varied, except between 12AM
 219 and 6AM. On total, our dataset comprises the time series of 34 banana presentations, 36 wine
 220 presentations, and 30 baseline samples. To implement online discrimination, the data was
 221 organized in moving windows with lengths of 10 minutes. For instance, for a presentation of
 222 length 60 min we create a total of $60 - 10 = 50$ windows to be used during the classification.

223 To solve the classification problem, we used a nonlinear classifier called Inhibitory Support

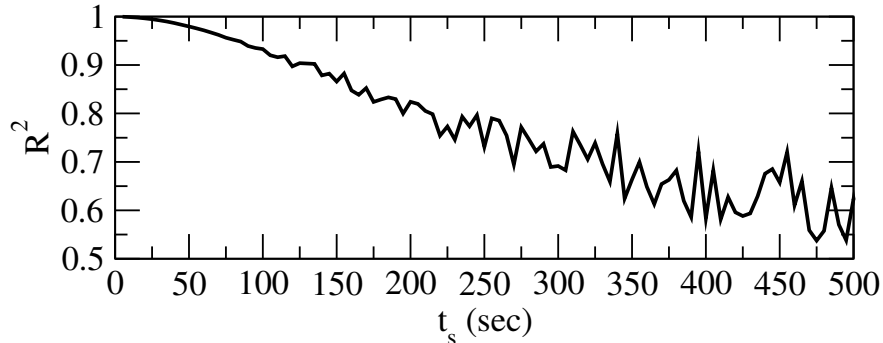


Figure 6: Average R^2 performance for increasing values of the sampling rate using 3 months of training and testing in the following month. Beyond the two minute sampling rate the R^2 drops below 0.9.

224 Vector Machine (ISVM) [33], which, in contrast to other multiclass SVM methods, is Bayes
225 consistent for three classes. ISVM is a particular case of the λ -SVM classifier, a pointwise
226 Fisher consistent multiclass classifier [34]. ISVMs have been successfully applied to arrays of
227 electronic noses (identical to the one used in the present paper) in controlled conditions [35,
228 34], in wind tunnel testing [26], and for ethylene discrimination in binary gas mixtures
229 [27]. Inspired by the learning mechanisms present in the insect brain [36], Inhibitory SVMs
230 use a large-margin classifier framework coupled to a mechanism of mutual and unselective
231 inhibition among classes. This mutual inhibition creates a competition, from which only one
232 class emerges. The decision function of Inhibitory SVMs associated with the j -th class and
233 the input pattern \mathbf{x}_i is defined as $f_j(\mathbf{x}_i) = \langle \mathbf{w}_j, \Phi(\mathbf{x}_i) \rangle - \mu \sum_{k=1}^L \langle \mathbf{w}_k, \Phi(\mathbf{x}_i) \rangle$, where L is
234 the number of classes and μ scales how strong each class will inhibit each other. If $\mu = 0$,
235 the decision function for standard SVMs is recovered. It can be analytically shown that the
236 optimal value for μ is $1/L$. The predicted class of a data point \mathbf{x}_i is determined by the
237 maximum among the decision functions for each class: $y(\mathbf{x}_i) = \arg \max_j f_j(\mathbf{x}_i)$. Because we
238 used Radial Basis Functions (RBF) as the kernel of the inhibitory SVM, our classifier had
239 two meta-parameters: the soft margin penalization C , and the inverse of the scale of the
240 RBF function γ . For more details about the ISVM model, see [33, 34].

241 To evaluate the impact on discrimination performance due to decorrelating the signals
242 from temperature and humidity sensors, we tested 4 different feature sets: raw sensor time
243 series (RS), raw sensor data with humidity and temperature (RS,T,H), filtered data (FS) by

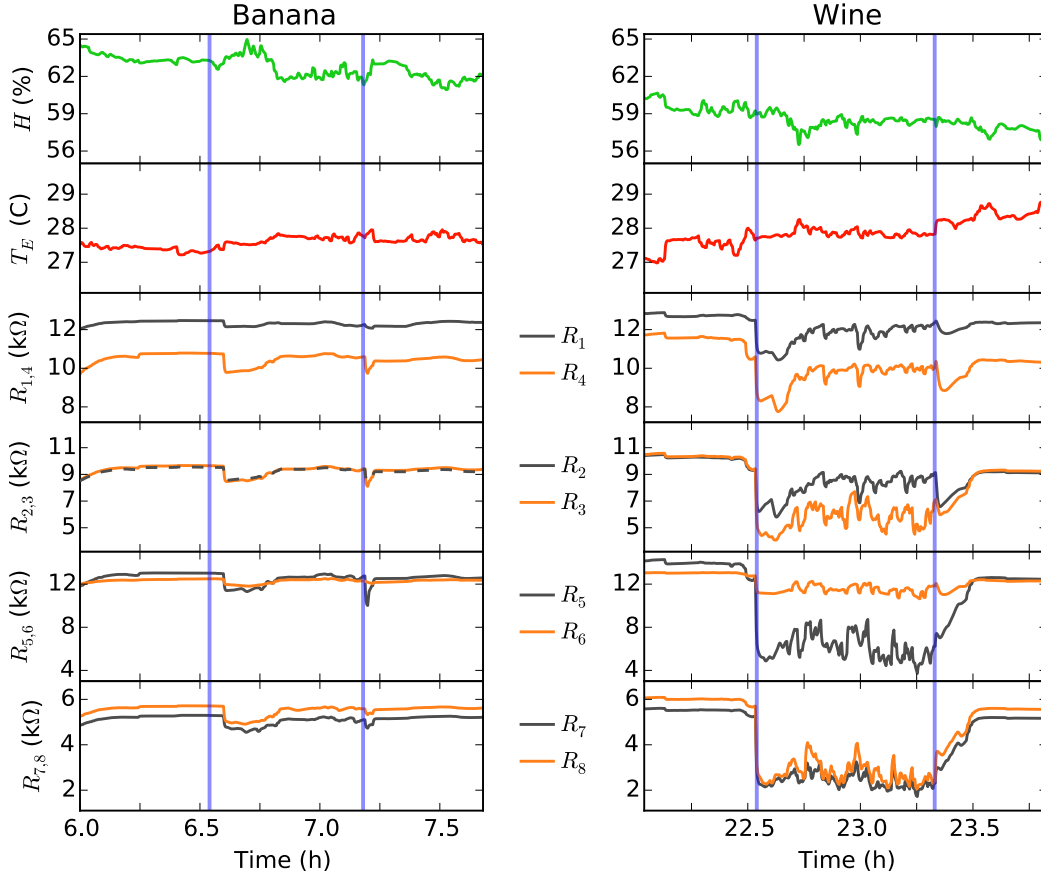


Figure 7: Example of response of all sensors due to the presentation of our stimuli: banana and wine. Sensors are indexed according to table 1. Vertical blue lines delimit the period of time that the stimulus remained close to the electronic nose. These time series were recorded on September 22nd, 2015.

244 decorrelating sensors using equation 6, and raw sensor data with filtered sensor data (RS,FS).
 245 To properly estimate the generalization ability of the model, we used standard procedures in
 246 machine learning to evaluate the performance of our classifier when discriminating samples
 247 not used for training the classifier [37]. We first divided our data set into two groups: a
 248 training set with 4/5th of the experimental presentations, and a test set with 1/5th of the
 249 data. All moving windows associated with the same presentations were kept in the same
 250 group. We used 4-fold cross-validation on the training set to estimate the classifier meta-
 251 parameters (C and γ). Using these meta-parameters, we re-trained the model using the
 252 whole training set and, then, assessed the performance using the test set. The range of

Feature set	Cross-validated accuracy	Accuracy in test	Std	p-value
RS	78.5%	76.5%	6.8%	0.02*
RS,T,H	73.3%	71.1%	6.8%	$1 \cdot 10^{-12}$ **
FS	72.4%	71.2%	4.8%	$2 \cdot 10^{-12}$ **
RS,FS	82.6%	80.9%	6.3%	1

Table 3: Classification accuracies in four feature sets (abbreviations are defined in the text) derived from our dataset with three classes: wine, banana, and baseline activity. The meta-parameters of the final Inhibitory SVM model were selected as those with the best cross-validated accuracies in the training set (second column), and the generalization error of the final model was evaluated in the test set (third column). The standard deviation (*std*) for the test dataset is estimated over 50 random partitions. Accuracy results from (RS,FS) are significantly different from all other feature sets (p-values from Kolmogorov-Smirnoff tests, ** passes at 1%, * passes at 5%).

values for the meta-parameters explored during the 4-fold cross-validation in the training set were $\gamma = \{0.5, 1, 5, 10, 50, 100\}$, and $C = \{10^4, 10^5, 10^6, 10^7, 10^8, 10^9\}$. To obtain a good statistical estimate of the classification accuracy, we re-shuffled our data and repeated this procedure 50 times, which was enough for the average and variance to converge.

Using the raw sensor data combined with the filtered signals (RS,FS) improved significantly (Kolmogorov-Smirnov, $p < 0.025$) the performance in online discrimination (Table 3). The raw sensors data (RS) alone reached 76% of accuracy, and including the temperature and humidity information (RS,T,H) did not improve. This shows that the additional features are likely redundant. Probably due to loss of inter-dependencies among sensors (as anticipated in section 5), the filtered sensor data (FS) by itself underperformed RS. Still, the model becomes more consistent, with lower variance in its performance, than the models trained on (RS) and (RS,T,H). Indeed, using both raw and filtered time series (RS,FS) improved significantly the model performance and its consistency. Thus, this experiment illustrates that temperature and humidity filters can not only improve pattern recognition performance, but they can also improve model stability, which is especially challenging in chemical sensing [38–42].

7. Conclusions

Changes in humidity and temperature shape the responses of arrays of MOX sensors, which in turn modifies nonlinearly chemical signatures of different volatiles. Filtering changes

272 in the sensor responses due to changes in both humidity and temperature during sampling
273 represents a major improvement for complex machine learning and monitoring tasks. We
274 used a model based on semiconductor energy bands to express the nonlinear dependence
275 of sensor resistance with humidity and temperature variations in an electronic nose. The
276 model was designed to fit in simpler micro-controllers, removing all possible non-linearities
277 up to second order in the change of humidity and temperature, envisioning applications to
278 cost-efficient devices. We found that the most dominant terms are the change in humidity,
279 the quadratic term of the change in humidity, and the correlated variations of humidity
280 and temperature. We showed that the model provides robust corrections to the distortions
281 caused by environmental changes. Therefore, our level of approximation on the semiconduc-
282 tor energy band is an inexpensive solution for applications in online and continuous home
283 monitoring using chemical sensors.

284 Specifically, the coefficient of determination R^2 of our model when fitted to all the 537
285 days of sampling is remarkably close to 100%. The model predicts a particular dependence
286 between two of the coefficients that is consistently verified in all the tested sensors. We
287 also showed that the maximum sampling period to obtain a reliable filter of humidity and
288 temperature is of the order of 1 minute. The accuracy achieved with faster sampling rates
289 provides small gains, and it would require some overhead in wireless communication when
290 the corrections are done at the base station. Additionally, 3-month training window was
291 selected to ensure that R^2 is larger than 90% for all sensors and throughout the whole year.
292 With 3 months, the training dataset likely included enough number of training examples
293 (events and background) while the effect of long-term drift in the sensors was still weak to
294 degrade the trained models. Previous work using similar sensing units showed that models
295 trained in two-month windows keep high accuracy during the following two months [43].
296 Stability could probably be improved further if one selects longer training windows or by
297 coupling our strategy with already proposed strategies to counteract long-term sensor drift
298 [43, 39, 44].

299 We verified empirically the benefits of decorrelating humidity and temperature from the

300 sensors' response by applying it to a task of gas discrimination. We recorded the response
301 of the sensors when presented with either a banana or glass of wine. Then, we used a Bayes-
302 consistent classifier [34, 33] to discriminate between the presence of banana, presence of
303 wine, and baseline activity. To compare the performance of the classifier with and without
304 the decorrelation of humidity-temperature, four different subsets of data were created by
305 combining raw sensor responses, filtered sensor data, and temperature and humidity. Ex-
306 perimental results show that including the filtered data in the classification model improves
307 not only the discrimination capability of the model, but also its stability.

308 In summary, we have shown that simultaneous recordings of the humidity and the temper-
309 ature can be used to help extracting relevant chemical signatures. The online decorrelation
310 model proposed in this work was designed for online operation even in the simpler micro-
311 controllers available in the market, which is essential for cost-efficient devices. Additionally,
312 humidity sensors are extremely appealing due to a high correlation between humidity levels
313 and human perception of air quality [45, 46]. Thus, when combined with other techniques
314 [18, 35, 47, 27, 48, 49], our model is likely to significantly enhance the performance of chemical
315 detection systems, as for instance of home monitoring tasks. Our contribution thus empha-
316 sizes the importance of simultaneous recordings of humidity and temperature, and that their
317 use is computationally amenable in sensor boards using low-energy micro-controllers.

318 **Acknowledgments**

319 This work has been supported by the California Institute for Telecommunications and
320 Information Technology (CALIT2) under Grant Number 2014CSRO 136. JF acknowledges
321 the support of the Marie Curie Actions and the Agency for Business Competitiveness of
322 the Government of Catalonia (ACCIÓ) for the grant TECSPR15-1-0031; and the Spanish
323 MINECO program, grant TEC2014-59229-R (SIGVOL). RH, TM, and IR-L acknowledge the
324 partial support by 3^a Convocatoria de Proyectos de Cooperacion Interuniversitaria UAM-
325 Banco Santander con EEUU. NR would like to acknowledge partial support by ONR grant
326 N000141612252. TM acknowledges CNPq grant 234817/2014- 3 for partial support. We are
327 also thankful to Flavia Huerta who collected data examples during the summer of 2015.

328 **References**

- 329 [1] N. Barsan, U. Weimar, Conduction model of metal oxide gas sensors, *Journal of Elec-*
330 *troceramics* 7 (3) (2001) 143–167.
- 331 [2] N. Barsan, U. Weimar, Understanding the fundamental principles of metal oxide based
332 gas sensors; the example of CO sensing with SnO₂ sensors in the presence of humidity,
333 *Journal of Physics: Condensed Matter* 15 (20) (2003) R813.
- 334 [3] M. Hubner, C. Simion, A. Tomescu-Stanoiu, S. Pokhrel, N. Bârsan, U. Weimar, Influe-
335 nce of humidity on CO sensing with p-type CuO thick film gas sensors, *Sensors and*
336 *Actuators B: Chemical* 153 (2) (2011) 347–353.
- 337 [4] J. Morante, Chemical to electrical transduction mechanisms from single metal ox-
338 ide nanowire measurements: response time constant analysis, *Nanotechnology* 24 (44)
339 (2013) 444004.
- 340 [5] M. G. Buehler, M. A. Ryan, Temperature and humidity dependence of a polymer-based
341 gas sensor, in: *AeroSense'97*, International Society for Optics and Photonics, 1997, pp.
342 40–48.
- 343 [6] N. Yamazoe, Toward innovations of gas sensor technology, *Sensors and Actuators B:*
344 *Chemical* 108 (1) (2005) 2–14.
- 345 [7] A.-C. Romain, J. Nicolas, P. Andre, In situ measurement of olfactive pollution with
346 inorganic semiconductors: Limitations due to humidity and temperature influence, in:
347 *Seminars in Food analysis*, Vol. 2, 1997, pp. 283–296.
- 348 [8] F. Hossein-Babaei, V. Ghafarinia, Compensation for the drift-like terms caused by en-
349 vironmental fluctuations in the responses of chemoresistive gas sensors, *Sensors and*
350 *Actuators B: Chemical* 143 (2) (2010) 641–648.
- 351 [9] G. F. Fine, L. M. Cavanagh, A. Afonja, R. Binions, Metal oxide semi-conductor gas
352 sensors in environmental monitoring, *Sensors* 10 (6) (2010) 5469–5502.

- 353 [10] A. Oprea, J. Courbat, N. Bârsan, D. Briand, N. De Rooij, U. Weimar, Temperature,
354 humidity and gas sensors integrated on plastic foil for low power applications, *Sensors*
355 and *Actuators B: Chemical* 140 (1) (2009) 227–232.
- 356 [11] C. Wang, L. Yin, L. Zhang, D. Xiang, R. Gao, Metal oxide gas sensors: sensitivity and
357 influencing factors, *Sensors* 10 (3) (2010) 2088–2106.
- 358 [12] A.-C. Romain, D. Godefroid, M. Kuske, J. Nicolas, Monitoring the exhaust air of a
359 compost pile as a process variable with an e-nose, *Sensors and Actuators B: Chemical*
360 106 (1) (2005) 29–35.
- 361 [13] A.-C. Romain, J. Delva, J. Nicolas, Complementary approaches to measure environ-
362 mental odours emitted by landfill areas, *Sensors and Actuators B: Chemical* 131 (1)
363 (2008) 18–23.
- 364 [14] W. Bourgeois, A.-C. Romain, J. Nicolas, R. M. Stuetz, The use of sensor arrays for
365 environmental monitoring: interests and limitations, *J. Environ. Monit.* 5 (2003) 852–
366 860.
- 367 [15] M. Ogawa, T. Togawa, Monitoring daily activities and behaviors at home by using
368 brief sensors, in: *Microtechnologies in Medicine and Biology, 1st Annual International,*
369 *Conference On. 2000, IEEE, 2000, pp. 611–614.*
- 370 [16] T. Oyabu, H. Nanto, T. Onodera, Odor sensing characteristics of a lavatory in a general
371 domicile, *Sensors and Actuators B: Chemical* 77 (1) (2001) 1–6.
- 372 [17] T. Oyabu, A. Okada, O. Manninen, D.-D. Lee, Proposition of a survey device with odor
373 sensors for an elderly person, *Sensors and Actuators B: Chemical* 96 (1) (2003) 239–244.
- 374 [18] J. Fonollosa, I. Rodriguez-Lujan, A. V. Shevade, M. L. Homer, M. A. Ryan, R. Huerta,
375 Human activity monitoring using gas sensor arrays, *Sensors and Actuators B: Chemical*
376 199 (2014) 398–402.

- 377 [19] I. Rodriguez-Lujan, G. Bailador, C. Sanchez-Avila, A. Herrero, G. Vidal-de Miguel,
378 Analysis of pattern recognition and dimensionality reduction techniques for odor bio-
379 metrics, *Knowledge-Based Systems* 52 (2013) 279–289.
- 380 [20] P. Chatonnet, D. Dubourdieu, Using electronic odor sensors to discriminate among
381 oak barrel toasting levels, *Journal of agricultural and food chemistry* 47 (10) (1999)
382 4319–4322.
- 383 [21] A. Shevade, M. Homer, H. Zhou, A. Jewell, A. Kisor, K. Manatt, J. Torres, J. Soler,
384 S.-P. Yen, M. Ryan, et al., Development of the third generation JPL electronic nose for
385 international space station technology demonstration, Tech. rep., SAE Technical Paper
386 (2007).
- 387 [22] M. A. Ryan, H. Zhou, M. G. Buehler, K. S. Manatt, V. S. Mowrey, S. P. Jackson, A. K.
388 Kisor, A. V. Shevade, M. L. Homer, Monitoring space shuttle air quality using the jet
389 propulsion laboratory electronic nose, *Sensors Journal, IEEE* 4 (3) (2004) 337–347.
- 390 [23] A. Fort, M. Mugnaini, I. Pasquini, S. Rocchi, V. Vignoli, Modeling of the influence of
391 H₂O on metal oxide sensor responses to CO, *Sensors and Actuators B: Chemical* 159 (1)
392 (2011) 82–91.
- 393 [24] R. Piedrahita, Y. Xiang, N. Masson, J. Ortega, A. Collier, Y. Jiang, K. Li, R. Dick,
394 Q. Lv, M. Hannigan, et al., The next generation of low-cost personal air quality sen-
395 sors for quantitative exposure monitoring, *Atmospheric Measurement Techniques* 7 (10)
396 (2014) 3325–3336.
- 397 [25] H. Windischmann, P. Mark, A Model for the Operation of a Thin-Film SnO_x
398 Conductance-Modulation Carbon Monoxide Sensor, *Journal of the Electrochemical So-*
399 *ciety* 126 (4) (1979) 627–633.
- 400 [26] A. Vergara, J. Fonollosa, J. Mahiques, M. Trincavelli, N. Rulkov, R. Huerta, On the
401 performance of gas sensor arrays in open sampling systems using Inhibitory Support
402 Vector Machines, *Sensors and Actuators B: Chemical* 185 (2013) 462–477.

- 403 [27] J. Fonollosa, I. Rodríguez-Luján, M. Trincavelli, A. Vergara, R. Huerta, Chem-
404 ical discrimination in turbulent gas mixtures with mox sensors validated by gas
405 chromatography-mass spectrometry, *Sensors* 14 (10) (2014) 19336–19353.
- 406 [28] S. Cieszczyk, Sensors signal processing under influence of environmental disturbances,
407 *Przeład Elektrotechniczny* 4 (2013) 129–131.
- 408 [29] F. Herrero-Carrón, D. J. Yáñez, F. de Borja Rodríguez, P. Varona, An active, inverse
409 temperature modulation strategy for single sensor odorant classification, *Sensors and*
410 *Actuators B: Chemical* 206 (2015) 555–563.
- 411 [30] E. Llobet, E. L. Hines, J. W. Gardner, S. Franco, Non-destructive banana ripeness
412 determination using a neural network-based electronic nose, *Measurement Science and*
413 *Technology* 10 (6) (1999) 538.
- 414 [31] J. Lozano, J. Santos, M. Horrillo, Classification of white wine aromas with an electronic
415 nose, *Talanta* 67 (3) (2005) 610–616.
- 416 [32] C. Di Natale, F. A. Davide, A. D’Amico, P. Nelli, S. Groppelli, G. Sberveglieri, An
417 electronic nose for the recognition of the vineyard of a red wine, *Sensors and Actuators*
418 *B: Chemical* 33 (1) (1996) 83–88.
- 419 [33] R. Huerta, S. Vembu, J. M. Amigó, T. Nowotny, C. Elkan, Inhibition in Multiclass
420 Classification, *Neural Comput.* 24 (9) (2012) 2473–2507.
- 421 [34] I. Rodríguez-Lujan, R. Huerta, et al., A Fisher consistent multiclass loss function with
422 variable margin on positive examples, *Electronic Journal of Statistics* 9 (2) (2015) 2255–
423 2292.
- 424 [35] I. Rodríguez-Lujan, J. Fonollosa, A. Vergara, M. Homer, R. Huerta, On the calibra-
425 tion of sensor arrays for pattern recognition using the minimal number of experiments,
426 *Chemometrics and Intelligent Laboratory Systems* 130 (2014) 123–134.

- 427 [36] T. S. Mosqueiro, R. Huerta, Computational models to understand decision making and
428 pattern recognition in the insect brain, *Current Opinion in Insect Science* 6 (2014)
429 80–85.
- 430 [37] R. O. Duda, P. E. Hart, D. G. Stork, *Pattern classification*, John Wiley & Sons, 2012.
- 431 [38] A.-C. Romain, J. Nicolas, Long term stability of metal oxide-based gas sensors for e-nose
432 environmental applications: An overview, *Sensors and Actuators B: Chemical* 146 (2)
433 (2010) 502–506.
- 434 [39] M. Padilla, A. Perera, I. Montoliu, A. Chaudry, K. Persaud, S. Marco, Drift compen-
435 sation of gas sensor array data by Orthogonal Signal Correction, *Chemom. Intell. Lab.*
436 *Syst.* 100 (1) (2010) 28–35.
- 437 [40] S. D. Carlo, M. Falasconi, E. Sánchez, A. Scionti, G. Squillero, A. P. Tonda, Increasing
438 pattern recognition accuracy for chemical sensing by evolutionary based drift compen-
439 sation., *Pattern Recognit. Lett.* 32 (13) (2011) 1594–1603.
- 440 [41] A. Vergara, S. Vembu, T. Ayhan, M. A. Ryan, M. L. Homer, R. Huerta, Chemical gas
441 sensor drift compensation using classifier ensembles, *Sens. Actuators, B.* 166–167 (2012)
442 320–329.
- 443 [42] E. Martinelli, G. Magna, S. De Vito, R. Di Fuccio, G. Di Francia, A. Vergara, C. Di
444 Natale, An adaptive classification model based on the Artificial Immune System for
445 chemical sensor drift mitigation, *Sensors and Actuators B: Chemical* 177 (2013) 1017–
446 1026.
- 447 [43] A. Vergara, S. Vembu, T. Ayhan, M. A. Ryan, M. L. Homer, R. Huerta, Chemical gas
448 sensor drift compensation using classifier ensembles, *Sensors and Actuators B: Chemical*
449 166 (2012) 320–329.
- 450 [44] A. Ziyatdinov, S. Marco, A. Chaudry, K. Persaud, P. Caminal, A. Perera, Drift com-
451 pensation of gas sensor array data by common principal component analysis, *Sensors*
452 *and Actuators B: Chemical* 146 (2) (2010) 460–465.

- 453 [45] P. Wolkoff, S. K. Kjærgaard, The dichotomy of relative humidity on indoor air quality,
454 Environment International 33 (6) (2007) 850–857.
- 455 [46] L. Fang, G. Clausen, P. O. Fanger, Impact of Temperature and Humidity on Perception
456 of Indoor Air Quality During Immediate and Longer Whole-Body Exposures, Indoor
457 Air 8 (4) (1998) 276–284.
- 458 [47] J. Fonollosa, S. Sheik, R. Huerta, S. Marco, Reservoir computing compensates slow
459 response of chemosensor arrays exposed to fast varying gas concentrations in continuous
460 monitoring, Sensors and Actuators B: Chemical 215 (2015) 618–629.
- 461 [48] A. Diamond, M. Schmuker, A. Berna, S. Trowell, T. Nowotny, Classifying continuous,
462 real-time e-nose sensor data using a bio-inspired spiking network modelled on the insect
463 olfactory system, Bioinspiration & biomimetics 11 (2) (2016) 026002.
- 464 [49] T. Mosqueiro, M. Strube-Bloss, R. Tuma, R. Pinto, B. H. Smith, R. Huerta, Non-
465 parametric change point detection for spike trains, in: 2016 Annual Conference on
466 Information Science and Systems (CISS), IEEE, 2016, pp. 545–550.